

# STATE OF THE CLIMATE IN 2011

Special Supplement to the  
*Bulletin of the American Meteorological Society*  
Vol. 93, No. 7, July 2012



and Atlantic basins as well. The Indian Ocean was also fresher in the upper 200 m from 30°S to 10°S, and from 300 m to 1000 m in roughly the same latitude span. The latitude band from 45°S to 30°S was more saline down to 700 m, with a subsurface extension northward to almost 10°S that reaches as deep as 300 m. North of 10°S, most of the water column is more saline than the long-term mean. Much of the freshening in the Indian Ocean, outside high southern latitudes, is in the eastern Indian extending westward from the west coast of Australia (see Fig. 3.12). Comparing 2011 to 2010 (Fig. 3.16b), the freshening in the band 15°S–35°S was more intense between the two years than between 2009 and 2010 (Levitus et al. 2011), to depths of 500 m. In the western Indian Ocean, there was a large (> 0.2) increase in salinity from 20°S to the equator which is confined to the upper 200 m. In the North Indian Ocean, the eastern Arabian Sea and eastern Bay of Bengal were fresher compared to the year before (Fig. 3.12), with this freshening dominating the zonal mean salinity anomalies down to 400 m.

*g. Surface currents*—R. Lumpkin, G. Goni, and K. Dohan

This section describes ocean surface current changes, transports derived from ocean surface currents, and features such as rings inferred from surface currents. Surface currents are obtained from in situ and satellite (altimetry and wind) observations.

Near-surface currents are measured in situ by drogued satellite-tracked drifting buoys and by current meters on moored buoys (see Appendix 2 for specific dataset information). During 2011, the drifter array ranged in size from a minimum of 352 drogued buoys to a maximum of 576, with a median size of 416 drogued drifters (undrogued drifters continue to measure SST, but are subject to significant wind slippage; Niiler et al. 1987). The moored array included 36 buoys with current meters, all between 16°S and 21°N. These tropical moorings compose the TAO/TRITON (Pacific; 16 buoys with

current meters reporting in 2012), PIRATA (Atlantic; 6 buoys) and RAMA (Indian; 14 buoys) arrays.

Global fields of ocean currents are estimated using two methodologies, both using the AVISO Ssalto/Duacs multimission altimeter near-real time gridded product. The first is a synthesis of AVISO with in situ drifter measurements and reanalysis winds (Niiler et al. 2003), which adjusts the altimeter-derived geostrophic velocity anomalies to match the observed in situ eddy kinetic energy. The second is the purely satellite-based OSCAR (Ocean Surface Current Analyses-Real time) product, which uses AVISO altimetry, winds, SST, and the Rio05 mean dynamic topography (Rio and Hernandez 2004) to create 1/3°-resolution surface current maps averaged over the 0 m – 30 m layer of the ocean (Bonjean and Lagerloef 2002). In both cases, anomalies are calculated with respect to the time period 1992–2007. Ocean transports are derived from a combination of sea height anomaly (from altimetry) and climatological hydrography.

Global zonal current anomalies and changes in anomalies from 2010 are shown in Fig. 3.17 and discussed below for individual ocean basins.

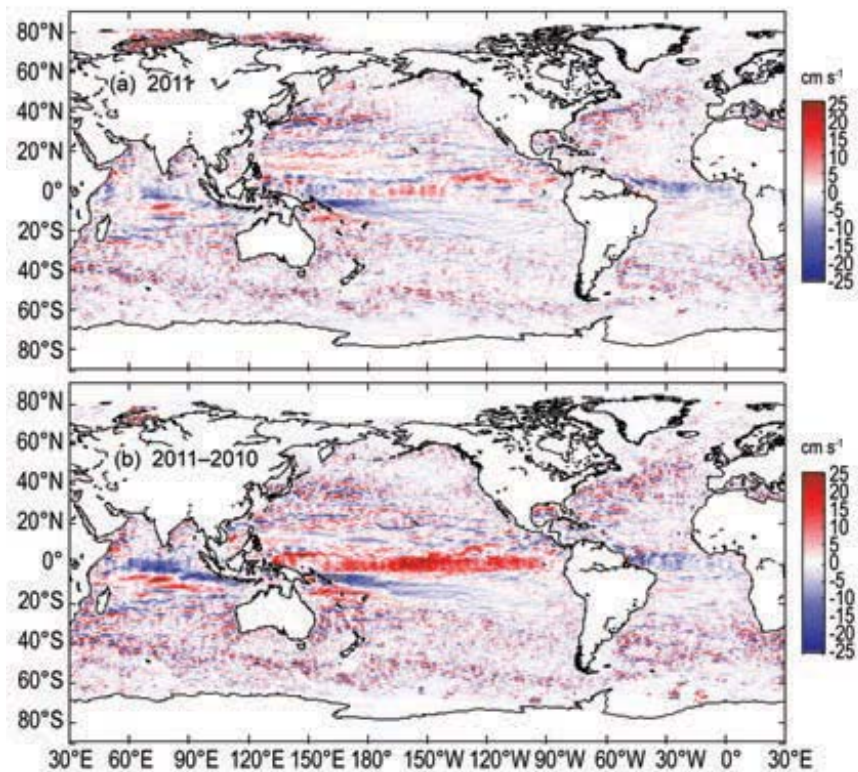


**FIG. 3.17. Global zonal geostrophic anomalies ( $\text{cm s}^{-1}$ ) for (a) 2011 and (b) 2011 minus 2010 derived from a synthesis of drifters, altimetry, and winds.**

### 1) PACIFIC OCEAN

In the tropical Pacific, 2011 began with surface currents near their climatological January values. This changed dramatically by February, however, with eastward anomalies developing from the South American coast to  $\sim 170^\circ\text{W}$ , with maxima of  $30\text{ cm s}^{-1} - 40\text{ cm s}^{-1}$  in the band  $100^\circ\text{W} - 150^\circ\text{W}$ . By March, the eastward equatorial anomalies spanned the basin. They persisted in strength in April, and then weakened quickly in May. By June, large-scale surface currents had returned to their climatological values. During the peak of this event in March–April, eastward anomalies peaked at  $30\text{ cm s}^{-1} - 40\text{ cm s}^{-1}$  at  $110^\circ\text{W}$  to  $170^\circ\text{E}$ . These surface current anomalies, with their associated advection of warm SST, acted to quickly erase the La Niña (cold) SST anomalies in the eastern tropical Pacific that had persisted since 2010 (Fig. 3.18; see also section 3b), yielding near-neutral values for the Niño 3, 3.4, and 4 indices by midyear.

In July 2011, westward equatorial anomalies of  $10\text{ cm s}^{-1} - 20\text{ cm s}^{-1}$  began developing at  $110^\circ\text{W} - 160^\circ\text{W}$ . This anomalous pattern expanded westward through August and September, at which point westward anomalies of  $15\text{ cm s}^{-1} - 20\text{ cm s}^{-1}$  were seen from  $\sim 100^\circ\text{W}$  to the western edge of the basin. By October, the pattern began weakening in the band  $160^\circ\text{W} - 170^\circ\text{E}$ , and by November the pattern was much patchier, with westward anomalies dominant only in the band  $90^\circ\text{W} - 160^\circ\text{W}$ . In December, westward

anomalies of  $15\text{ cm s}^{-1} - 25\text{ cm s}^{-1}$  again developed in the western Pacific, in the band  $130^\circ\text{W} - 160^\circ\text{E}$ .

Because of the alternating signs of zonal current anomalies in early vs. late 2011, annual mean zonal current anomalies (Fig. 3.17) are not as dramatic as they were in 2010 (a predominantly La Niña year for zonal current anomalies). The 2010 anomalies dominate 2011 minus 2010 (Fig. 3.17b).

Surface current anomalies in the equatorial Pacific typically lead SST anomalies by several months, with a magnitude that scales with the SST anomaly magnitude. Recovery to normal current conditions is also typically seen before SST returns to normal. Thus, current anomalies in this region are a valuable predictor of the evolution of SST anomalies and their related climate impacts. This leading nature can be seen clearly in the first principal empirical orthogonal function (EOF) of surface current (SC) anomaly and separately of SST anomaly in the tropical Pacific basin (Fig. 3.18). In the altimetry time period 1993–2011, the maximum correlation between SC and SST is  $R=0.68$  with SC leading SST by 81.1 days. In 2011, the most dramatic feature of this mode was the extremely rapid change in the SC anomaly from negative values in late 2010 to El Niño-like (positive) values in early 2011. This switch in the sign of the SC anomaly happened as the SST anomaly reached its strongest negative value (Fig. 3.18); for the next few months, while the SC anomaly remained positive, the negative SST anomaly decreased in magnitude. In the latter half of 2011, the SC anomaly returned to neutral-to-La Niña-like (negative) values, leading the return of cold SST anomalies by several months (Fig. 3.18). It is interesting to note that, unlike earlier years, a positive SST anomaly did not follow the positive SC anomaly in early 2011; this is likely due to the extreme magnitude of the 2010 La Niña SST anomaly (the most negative value in this time series) and the relatively brief duration of the positive SC anomaly in 2011.

In the *State of the Climate in 2010*, it was noted that the Kuroshio exhibited a narrower and stronger annual mean signature, and shifted approximately  $1^\circ$  in latitude to the north compared to 2006–09. This pattern continued through 2011, with no large-scale pattern in the 2011 minus 2010 difference (Fig. 3.17b) indicating a shift in

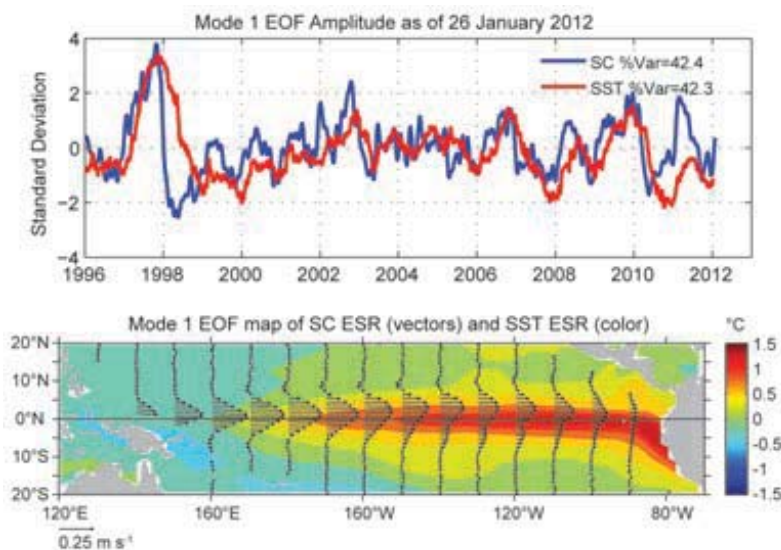


**FIG. 3.18. Principal empirical orthogonal functions (EOF) of surface current (SC) and SST anomaly variations in the tropical Pacific from the OSCAR model. (Top) Amplitude time series of the EOFs normalized by their respective standard deviations. (Bottom) Spatial structures of the EOFs.**

the Kuroshio Extension latitude with respect to 2010.

## 2) INDIAN OCEAN

In January 2011, westward equatorial anomalies of  $\sim 20 \text{ cm s}^{-1}$  were seen in the central Indian Ocean ( $75^\circ \text{E}$ – $90^\circ \text{E}$ ), north of a band of eastward anomalies at  $50^\circ \text{E}$ – $100^\circ \text{E}$ ,  $10^\circ \text{S}$ . The westward equatorial anomalies persisted through June, with the pattern shifting westward through this period. In July, eastward equatorial anomalies of  $10 \text{ cm s}^{-1}$  –  $20 \text{ cm s}^{-1}$  developed at  $60^\circ \text{E}$ – $85^\circ \text{E}$ ; this pattern weakened and shifted to the west in August, and was extremely weak in September when westward equatorial anomalies again developed in the center of the basin. These anomalies developed in intensity through November, reaching peak values of  $30 \text{ cm s}^{-1}$  –  $40 \text{ cm s}^{-1}$  in November at  $65^\circ \text{E}$ – $75^\circ \text{E}$ . They then rapidly weakened, and December saw a return to near-normal climatological surface current values across the basin at large scales. In the annual mean (Fig. 3.17), westward anomalies dominated the basin in 2011, in contrast to the weak eastward anomalies of 2010.

The shedding of eddies from the Agulhas Current into the Atlantic basin as seen in altimetry remained at its climatological value. The transport of the Agulhas can be estimated by combining sea height anomaly and climatological hydrography; in 2011, the transport of the Agulhas decreased by  $\sim 5 \text{ Sv}$  (Sverdrup, equal to  $10^6 \text{ m}^3 \text{ s}^{-1}$ , a unit commonly used for ocean volume transports) with respect to the 2010 mean, with much weaker values seen for the second half of 2011 (Fig. 3.19). A dramatic, brief maximum of  $84 \text{ Sv}$  was observed at the beginning of 2011, exceeding all previous maxima observed since 1993.

## 3) ATLANTIC OCEAN

In the first few months of 2011, the tropical Atlantic basin did not exhibit any basin-wide zonal surface current anomalies, although westward anomalies tended to dominate near the equatorial band east of  $\sim 30^\circ \text{W}$ . Through boreal spring to summer, these relatively weak westward equatorial anomalies expanded across the basin. These anomalies persisted through September and October, and intensified in

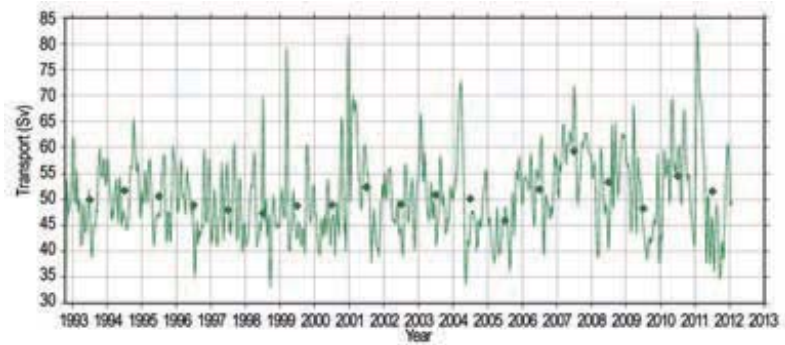


**FIG. 3.19. Transport of the Agulhas Current from a combination of sea height anomaly and climatological hydrography (<http://www.aoml.noaa.gov/phod/altimetry/cvar/agu/index.php>).**

November to  $10 \text{ cm s}^{-1}$  –  $20 \text{ cm s}^{-1}$  at  $20^\circ \text{W}$ – $30^\circ \text{W}$ . The overall annual mean anomaly (Fig. 3.17) was westward in 2011, similar to the 2010 pattern.

In the Gulf of Mexico, surface current speed anomalies of  $30 \text{ cm s}^{-1}$  –  $35 \text{ cm s}^{-1}$  were present along and north of the climatological Loop Current path in 2011. An overall increase in the Loop Current strength is not likely, as the measured transport of the Florida Current between Florida and the Bahamas increased by less than  $1 \text{ Sv}$  between 2010 and 2011 (see section 3h). Thus, this pattern suggests that the Loop Current penetrated farther north on average during 2011.

The North Brazil Current, which sheds rings that carry waters from the South Atlantic Ocean into the North Atlantic, continued to exhibit anomalous behavior as reported in the *State of the Climate in 2010* report (Fig. 3.20). Sea heights associated with the current and rings continued having the large values observed in 2010; and seven rings were identified to shed. Transport values of this current and its retro-reflection remained average during 2011.

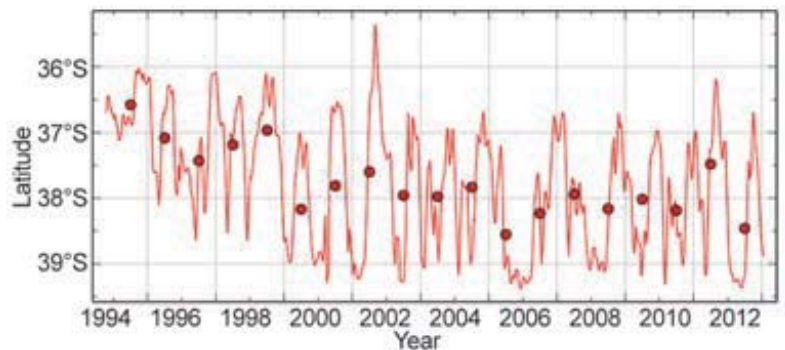


**FIG. 3.20. Position of the Brazil-Malvinas front at its separation from the South American continental shelf break, resolved by the change in sea height across the front ([http://www.aoml.noaa.gov/phod/altimetry/cvar/mal/BM\\_ts.php](http://www.aoml.noaa.gov/phod/altimetry/cvar/mal/BM_ts.php)). The solid line is a 28-day running average; dots indicate annual averages.**

Against the east coast of South America, the southward-flowing warm, salty Brazil Current meets the northward flowing cold, fresh Malvinas Current to create the Confluence Front. During 2011, the separation of the front from the continental shelf break continued to exhibit annual periodicity driven by wind stress curl variations (cf., Goni and Wainer 2001). The annual mean position of the front in 2011 was 38.5°S, a shift to the south from the 37.5°S position in 2010. This location is as far south as the annually-averaged front has been seen since the launch of the TOPEX/Poseidon altimeter in 1992, and was matched by only one other year (2004). Since 1992, the front has shifted significantly southward in response to wind stress curl changes driven by SST anomalies advected from the Indian Ocean (Lumpkin and Garzoli 2010; Goni et al. 2011).

*h. Meridional overturning circulation observations in the subtropical North Atlantic*—M. O. Baringer, S. A. Cunningham, C. S. Meinen, S. Garzoli, J. Willis, M. Lankhorst, A. Macdonald, U. Send, W. R. Hobbs, E. Frajka-Williams, T. O. Kanzow, D. Rayner, W. E. Johns, and J. Marotzke

For several years, this section has reported on the meridional redistribution of mass associated with the large-scale vertical circulation within ocean known as the meridional overturning circulation (MOC). Here, the MOC is defined as the maximum of the vertically integrated basin-wide stream function, which changes as a function of latitude and time and is influenced by many physical systems embedded within it. It is related to the meridional transport of heat (MHT) in the oceans, although the relationship may not be direct and can vary with latitude; for example, where horizontal gyre circulation is strong, the heat transport can largely be ascribed to the wind-driven circulation. Variability in oceanic MHT can in turn contribute to heat storage, sea-level rise, and air-sea fluxes and hence influence local climate on land. Therefore, closing the ocean heat budget is a central area of study for understanding and predicting societally-relevant impacts from the oceans. Changes in MOC and MHT can be inferred from “fingerprint” changes in ocean temperature, sea-level rise, and changes in individual current systems (see Baringer et al. 2011 and previous *State of*

*the Climate* reports for more discussion). This annual report focuses on the longest time series observations of ocean heat and mass transport currently available and what can be inferred from them about the current state of the MOC and MHT.

Recommendations for a coordinated observing system to begin to measure MOC were presented at the international conference OceanObs’09 in September 2009 (e.g., Cunningham et al. 2010; Rintoul et al. 2010) and subsequent planning workshops focused on expanding existing observations to include the subpolar North and South Atlantic (e.g., Garzoli et al. 2010). The most complete MOC observing system has been in place since April 2004, and spans the subtropical gyre in the North Atlantic near 26.5°N. The system is composed of UK-NERC RAPID-WATCH moorings, US-NSF Meridional Overturning Circulation Heat-Transport Array (MOCHA), and the US-NOAA Western Boundary Time Series program (see also Rayner et al. 2010; Chidichimo et al. 2010).

The estimates of MOC from the 26.5°N array include data from April 2004 to December 2010 (see also Rayner et al. 2010), shown in Fig. 3.21. Over this

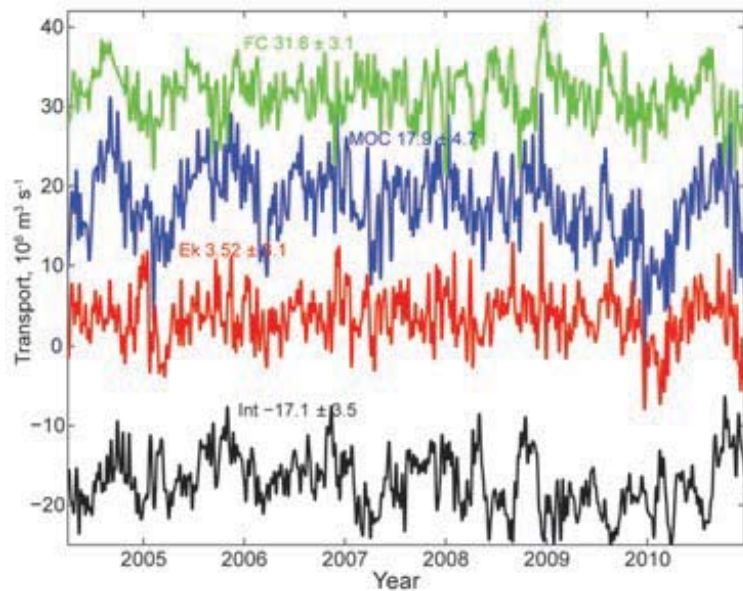


**FIG. 3.21.** Daily estimates of the strength of the meridional overturning circulation (MOC; blue line) and its components, the Florida Current (FC; green), wind-driven Ekman transport (Ek; red), and the geostrophic interior (Int; black), as measured by the UK National Environmental Research Council Rapid Climate Change Program, the National Science Foundation’s Meridional Overturning and Heat transport Array, and the NOAA Western Boundary Time Series Program. The interior volume transport estimate (accurate to 1 Sv, Cunningham et al. 2007) is based on the upper ocean transport from April 2004 to December 2010 (see also Rayner et al. 2010; Kanzow et al. 2010), with a 10-day low pass filter applied to the daily transport values.